This is the author's version of a work that was accepted for publication in the following source:

Abbott, Carla J., David A. X. Nayagam, Chi D. Luu, Stephanie B. Epp, Richard A. Williams, Cesar M. Salinas-LaRosa, Joel Villalobos, Ceara McGowan, Mohit N. Shivdasani, Owen Burns, Jason Leavens, Jonathan Yeoh, Alice A. Brandli, Patrick C. Thien, Jenny Zhou, Helen Feng, Chris E. Williams, Robert K. Shepherd, and Penelope J. Allen. 2018. Safety Studies for a 44-Channel Suprachoroidal Retinal Prosthesis: A Chronic Passive Study. *Investigative Ophthalmology & Visual Science*. **59**(3): 1410-1424.

Notice: Changes introduced as a result of publishing processes such as copy-editing and formatting may not be reflected in this document. For a definitive version of this work, please refer to the published source.

The final publication is available at:

https://iovs.arvojournals.org/article.aspx?articleid=2675236

Copyright of this article belongs to: © 2018 The Authors

This work is licensed under a Creative Commons Attribution-NonCommercial-NoDerivatives 4.0 International License.

Safety Studies for a 44-Channel Suprachoroidal Retinal Prosthesis: A Chronic Passive Study

Carla J. Abbott,[1,2] David A. X. Nayagam,[3,4] Chi D. Luu,[1,2] Stephanie B. Epp,[3] Richard A. Williams,[4,5] Cesar M. Salinas-LaRosa,[4,5] Joel Villalobos,[3] Ceara McGowan,[3] Mohit N. Shivdasani,[3,6] Owen Burns,[3] Jason Leavens,[7] Jonathan Yeoh,[1,2] Alice A. Brandli,[1,8] Patrick C. Thien,[3,9] Jenny Zhou,[3] Helen Feng,[3] Chris E. Williams,[3,9] Robert K. Shepherd,[3,9] and Penelope J. Allen[1,2]

[1]Centre for Eye Research Australia, Royal Victorian Eye and Ear Hospital, East Melbourne, Australia
[2]Department of Surgery (Ophthalmology), University of Melbourne, Australia
[3]Bionics Institute, East Melbourne, Australia
[4]Department of Pathology, University of Melbourne, Australia
[5]St. Vincent's Hospital Melbourne, Fitzroy, Australia
[6]Graduate School of Biomedical Engineering, University of New South Wales, Australia
[7]Cochlear Ltd., Sydney, Australia
[8]Department of Anatomy and Neuroscience, University of Melbourne, Australia
[9]Medical Bionics Department, University of Melbourne, Australia

Correspondence: Carla J. Abbott, Centre for Eye Research Australia, Level 7 Peter Howson Wing, 32 Gisborne Street, East Melbourne, VIC 3002, Australia; c.abbott@unimelb.edu.au.

Submitted: September 30, 2017
Accepted: February 1, 2018

Citation: Abbott CJ, Nayagam DAX, Luu CD, et al. Safety studies for a 44-channel suprachoroidal retinal prosthesis: a chronic passive study. *Invest Ophthalmol Vis Sci*. 2018;59:1410–1424. https://doi.org/10.1167/iovs.17-23086

Purpose. Following successful clinical outcomes of the prototype suprachoroidal retinal prosthesis, Bionic Vision Australia has developed an upgraded 44-channel suprachoroidal retinal prosthesis to provide a wider field of view and more phosphenes. The aim was to evaluate the preclinical passive safety characteristics of the upgraded electrode array.

Methods. Ten normal-sighted felines were unilaterally implanted with an array containing platinum electrodes (44 stimulating and 2 returns) on a silicone carrier near the area centralis. Clinical assessments (color fundus photos, optical coherence tomography, full-field electroretinography, intraocular pressure) were performed under anesthesia prior to surgery, and longitudinally for up to 20 weeks. Histopathology grading of fibrosis and inflammation was performed in two animals at 13 to 15 weeks.

Results. Eight animals showed safe electrode array insertion (good retinal health) and good conformability of the array to the retinal curvature. Eight animals demonstrated good mechanical stability of the array with only minor (<2 disc diameters) lateral movement. Four cases of surgical or stability complications occurred due to (1) bulged choroid during surgery, (2) hemorrhage from a systemic bleeding disorder, (3) infection, and (4) partial erosion of thin posterior sclera. There was no change in retinal structure or function (other than that seen at surgery) at endpoint. Histopathology showed a mild foreign body response. Electrodes were intact on electrode array removal.

Conclusions. The 44-channel suprachoroidal electrode array has an acceptable passive safety profile to proceed to clinical trial. The safety profile is expected to improve in human studies, as the complications seen are specific to limitations (anatomic differences) with the feline model.

Keywords: retinal prosthesis, optical coherence tomography, electroretinography, retinal histology, retinal safety

Retinal prostheses can restore some functional vision to patients with profound vision loss from progressive retinal degenerative diseases such as retinitis pigmentosa.[1–4] Retinitis pigmentosa affects over 1.5 million people worldwide, and is the leading cause of irreversible vision loss in a working age population.[5] Retinal prostheses bypass the degenerating photoreceptors and electrically stimulate the remaining intact neurons in the inner retina, including the bipolar cells and the retinal ganglion cells.

There are three retinal prostheses currently commercially available (Argus II device; Second Sight Medical Products, Sylmar, CA, USA[6]; Alpha IMS and AMS devices; Retina Implant AG, Reutlingen, Germany[7]; and IRIS VRS; Pixium Vision, Paris, France[8,9]), and further devices are at various stages of development by other groups.[10–16] These devices are designed for implantation in epiretinal,[6,9,10] subretinal,[11–13,17] suprachoroidal,[16] and intrascleral[14,15] locations. However, intraocular serious adverse events (SAEs) relating to the stability of the electrode array, conjunctival and scleral erosions, retinal detachment, hypotony, and endophthalmitis have been associated with epiretinal implants[6,17–21] and SAEs relating to raised intraocular pressure (IOP), and retinal detachment have

Copyright 2018 The Authors

This work is licensed under a Creative Commons Attribution-NonCommercial-NoDerivatives 4.0 International License.

Downloaded From: https://iovs.arvojournals.org/pdfaccess.ashx?url=/data/journals/iovs/936793/ on 03/19/2018

Table 1. Comparison of Electrode Array Design Between The Prototype Preclinical Devices Used in Previous Passive[27] and Active[28] Chronic Studies, The First In-Human Clinical Trial,[24] and the Current Preclinical 44-Channel Study

Design Components	Prototype Passive Preclinical[27]	Prototype Active Preclinical[28]	Prototype Clinical[24]	44-Channel Preclinical
Platinum electrodes*	21 × Ø 0.6 mm 2 × Ø 2.0 mm	12 × Ø 0.6 mm 2 × Ø 2.0 mm	30 × Ø 0.6 mm 3 × Ø 0.4 mm 2 × Ø 2.0 mm	44 × Ø 1.0 mm 2 × Ø 2.0 mm
Silicone carrier dimensions	19 × 8 mm	17 × 8 mm	19 × 8 mm	17 × 8.5 mm
Maximum carrier thickness	1.0 mm	1.0 mm	1.0 mm	0.6 mm
Lead-wire cable	Ø 1.2 mm; 23 wires	Ø 1.2 mm; 14 wires	Ø 1.2 mm; 23 wires†	Ø 1.2 mm; 48 wires‡

Ø, diameter.
* Diameters of electrodes refer to the exposed surface area and physical electrode areas may be slightly larger.
† Comprised one wire from each of 20 stimulating electrodes and three return electrodes.
‡ Comprised one wire from each of 44 stimulating electrodes and two wires from each of two return electrodes.

occurred with subretinal implants.[7,17,21–23] These SAEs are generally related to the complex surgical procedures required for epiretinal and subretinal placement and often require further surgical or medical intervention. Previous studies with suprachoroidal-[24] and intrascleral-[15] based devices shows no evidence of intraocular SAE's, although long-term safety for greater than 1 year has not yet been evaluated. Despite the electrode arrays in suprachoroidal and intrascleral devices being located more distal to the inner retinal target cells than epiretinal and subretinal implants, they can readily generate phosphene vision in late-stage retinitis pigmentosa patients.[15,24–26]

In 2012, we conducted a Phase 1 clinical trial (Clinicaltrials.gov NCT01603576) using a prototype suprachoroidal retinal prosthesis in three patients with end-stage retinitis pigmentosa, and demonstrated that the surgical procedure was safe (no intraocular SAEs), the device position was stable over time, and repeatable phosphene percepts were elicited in all subjects.[24] At the conclusion of the trial, we received feedback from the patients that they would prefer an increased number of phosphenes and an increased visual field in a next-generation retinal prosthesis. Hence, we have now upgraded the retinal prosthesis to a 44-channel electrode array, both increasing the number of electrodes and the field of view. There are two key design changes from our previous prototype arrays[24,27,28] that alter the mechanical characteristics of the retinal prosthesis (1) an increase in metal to silicone carrier ratio, and (2) an increase in the number of wires in the lead-wire cable. Hence, we determined it was critical to perform a preclinical passive chronic safety study to determine the surgical safety, stability, conformability, robustness, and biocompatibility of this upgraded 44-channel electrode array, prior to proceeding to clinical trial.

Methods

Subjects and Ethics Statement

Ten adult normally sighted cats, weighing between 2.6 and 5.7 kg on the day of monocular implant surgery, were the subjects of this study. The 44-channel electrode array design was an iterative process, involving implantation in a total of 28 animals as part of a wider study, but only the 10 animals implanted with the final array design were included in this study. A companion publication will further detail the iterative electrode array design and engineering process. Cats were chosen as our large-eye model to assess retinal safety of our retinal prosthesis as they have a similar axial length and retinal structure and function to humans,[29] and to allow comparison to our previous preclinical safety studies performed with the prototype electrode array. All procedures were approved and monitored by the Bionics Institute Animal Research Ethics Committee (AREC#15/324AB and AREC#16/341AB) and complied with the National Health and Medical Research Council's "Australian code for the care and use of animals for scientific purposes" (2013) and "Guidelines on the Care of Cats Used for Scientific Purposes" plus the Victorian State (Australia) "Prevention of Cruelty to Animals' Act" (1986 and amendments), and the ARVO Statement for the Use of Animals in Ophthalmic and Vision Research. All procedures (surgeries and noninvasive follow-up assessments) were carried out under anesthesia and all efforts were made to minimize suffering.

44-Channel Suprachoroidal Electrode Array Design

In the upgraded 44-channel electrode array design compared with the previous prototype designs, the metal density, or ratio to silicone has increased due to an increased number of electrodes, a larger electrode diameter and a thinner silicone carrier (Table 1). Furthermore, the metal density of the lead-wire cable (90% platinum–10% iridium) has increased due to more wires contained within the same total outer diameter. These mechanical changes may have an effect on ease of surgical insertion, long-term stability, conformability, and robustness of the electrode array. Figure 1 shows a diagram of the 44-channel electrode array and lead-wire cable compared with the previous preclinical prototype designs.[24,27,28] The total electrode number was increased to 46 platinum electrodes (of which 2 were the larger diameter return electrodes) within the 17 × 8.5-mm medical-grade silicone carrier (mixture of MED-4860 and either MED-1540 or MED-4830 liquid silicone; NuSil Technology, Carpinteria, CA, USA) to increase number of phosphenes and field of view without adding to the overall footprint. The electrode diameter was increased to 1 mm to reduce the charge density for stimulation safety purposes.[30] The thickness of the silicone carrier was reduced to compensate for the higher metal content and to reduce overall stiffness. The orientation of the returns was altered (Fig. 1), which also has a local impact on stiffness in this region of the electrode array. A patch to stabilize the electrode array, attach the lead-wire cable, and cover the scleral incision was located over the scleral exit point (MEDIFAB 07-105/52, Art No. 051032460000; SEFAR Mesh & Technology, Blacktown, NSW, Australia) and a second patch to anchor the lead-wire cable was located at the orbital margin point (Fig. 1). The electrode arrays were cleaned in an ultrasonic cleaner as follows: (1) double-distilled water (ddH_2O) for 10 minutes, (2) detergent solution (ddH_2O + Pyroneg; Diversey Australia Pty. Ltd., New South Whales, Australia) for 10 minutes, (3) ddH_2O 2 × 5 minutes, (4) 100%

Investigative Ophthalmology & Visual Science

Downloaded From: https://iovs.arvojournals.org/pdfaccess.ashx?url=/data/journals/iovs/936793/ on 03/19/2018

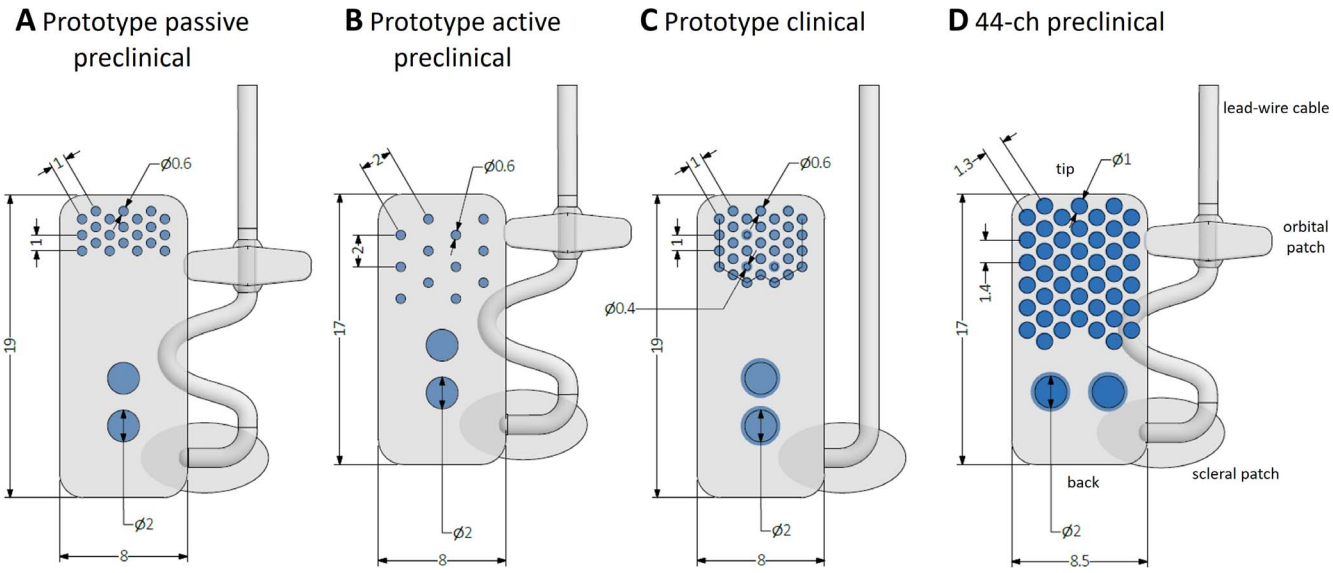

FIGURE 1. Comparison of suprachoroidal electrode array designs. (**A**) The prototype design used in the preclinical passive chronic study[27] prior to the first in-human prototype clinical trial. (**B**) The prototype design used in the preclinical active chronic study[28] prior to the first in-human prototype clinical trial. (**C**) The first in-human clinical prototype design.[24] (**D**) The 44-channel electrode array used in the current preclinical study. There are 44 × Ø 1.0-mm platinum stimulating electrodes and 2 × Ø 2.0-mm platinum return electrodes in a 17 × 8.5-mm silicone carrier. The scleral and orbital margin fixation patches were used to anchor the implant and lead-wire cable. Ø, diameter.

ethanol for 5 minutes, and (5) ddH_2O 2 × 5 minutes. They were subsequently autoclaved at a maximum of 134°C for 1 hour, stored under sterile conditions, and rinsed in sterile saline immediately prior to surgery.

Experimental Design

The study design was for 10 animals to be implanted with the 44-channel preclinical electrode array for at least 12 weeks. A mixed cohort with passive (sham) implantation and active electrical stimulation was planned to minimize the total number of animals required. Of the 10 total animals, two animals did not receive electrical stimulation and were evaluated longitudinally with clinical techniques in addition to histopathology after 13 to 15 weeks of implantation. The remaining eight animals received electrical stimulation from 4 weeks postsurgery onward using the electrical stimulation system described previously.[31] These eight animals were also monitored longitudinally with clinical techniques, and the passive implantation outcomes pertaining to implantation safety, device stability, electrode array conformability, and electrode robustness are reported here. The electrical stimulation safety outcomes including retinal thickness and histopathology from the active stimulation subcohort will be presented in a companion publication.

Surgery and Postoperative Care

Vitreoretinal surgeons under aseptic conditions performed the surgeries. Animals were anesthetized with an initial dose of xylazine (2 mg/kg subcutaneous [s.c.]) and ketamine (20 mg/kg s.c. or intramuscular [i.m.]), then maintained with a continuous flow of 1% to 2% isoflurane (IsoFlo; Abbott Laboratories, North Chicago, IL, USA) , in oxygen through an endotracheal tube for the duration of the surgery. Animals were intubated, body temperature maintained with a heat pad at 37°C, and breathing, heart rate, oxygen saturation, and blood pressure were monitored continuously (Cardell veterinary monitor 9405; Casmed Medical Systems, Branford, CT, USA). Hartmann's solution was administered (intravenous [i.v.] or s.c.) as a fluid supplement and ocular lubricant (HPMC PAA gel; Alcon, Macquarie Park, NSW, Australia) was instilled to prevent corneal desiccation. Mydriasis was induced in the eye being operated on with 1% tropicamide, 10% phenylephrine hydrochloride, and 1% atropine (Bausch & Lomb, Chatswood, NSW, Australia).

The surgical method of electrode array implantation is shown diagrammatically in previous publications.[27,32] The detailed surgical implantation method of the whole electrical stimulation system including an x-ray fluoroscopy of the implanted eye has also been described previously.[28] In brief, a lateral canthotomy and conjunctival peritomy were performed, prior to a 9-mm scleral incision located at 5-mm posterior and parallel to the limbus. The incision is more anterior in cat than in human surgery,[33] where it is positioned underneath the lateral rectus muscle, because the cat sclera is substantially thinner posteriorly. The superior margin of the incision was extended posteriorly as an "L" to enable the cable exiting the eye to sit flat on the sclera. A crescent knife (Alcon Laboratories) and lens glide (Beaver Visitec International, Waltham, MA, USA) were used to open the suprachoroidal space, then the array was advanced into the suprachoroidal pocket to be positioned under the superior-temporal retina close to the area centralis, taking care to avoid the long-posterior ciliary arteries. The implant position under the retina was photographed with a fundus lens (Volk Quadraspheric, Mentor, OH, USA) and surgical microscope (Zeiss OPMI 6-CFR XY; Carl Zeiss AG, Oberkochen, Germany). The scleral wound was closed with 5/0 and 8/0 nylon sutures and the scleral patch was sutured to the sclera overlying the wound with 8/0 nylon sutures to protect it and anchor the array. The conjunctiva was closed with 8/0 vicryl sutures and ocular lubricant instilled. The lead-wire cable was looped posteriorly in the episcleral space and the orbital patch was sutured with 5/0 nylon sutures as a secondary anchor point onto the zygomatic process. In animals with a passive array ($N = 2$), the lead-wire cable end was positioned subcutaneously superorostral to the pinna and the skin closed with 5/0 and 6/0 vicryl and 5/0 nylon sutures.[27] In animals with an electrode array intended for chronic electrical stimulation ($N = 8$), the

Investigative Ophthalmology & Visual Science

Downloaded From: https://iovs.arvojournals.org/pdfaccess.ashx?url=/data/journals/iovs/936793/ on 03/19/2018

lead-wire cable was routed subcutaneously, secured to the skull, and had a percutaneous connector exiting at a wound between the scapulae.[28]

Analgesia was provided with a nonsteroidal anti-inflammatory agent (carprofen 4 mg/kg s.c.; Norbrook, Newry, Northern Ireland) immediately postsurgery (day 0), followed by the opioid buprenorphine (0.01 mg/kg s.c.; Temgesic, Reckitt Benckiser, Sydney, Australia) twice on day 1 and once on day 2. Prophylactic systemic antibiotic was provided (Clavulox, 10 mg/kg s.c. or 12.5 mg/kg bid PO; Pfizer Italia, Rome, Italy) immediately after surgery, then daily for 7 days. Prophylactic topical antibiotic (chloramphenicol 0.5%; Chlorsig, Sigma Pharmaceuticals, VIC, Australia) and topical steroid (prednefrin forte 1%; Sigma Pharmaceuticals, VIC, Australia) was applied to the eye four times a day for 14 days. In two animals (16_321, 16_527) topical steroid was continued twice a day for a further 14 days according to surgical advice.

In Vivo Clinical Assessments

Noninvasive clinical assessment tools were used to assess structural and functional status of the retina both following implantation surgery and over the chronic implantation period, electrode array stability and conformability to the retinal curvature, and electrode tilt relative to retinal curvature. Animals were anesthetized with an initial dose of xylazine (2 mg/kg s.c.) and ketamine (20 mg/kg s.c. or i.m.), then maintained with ketamine i.m. at one-third the original dose as required. Topical tropicamide 1% (Bausch & Lomb, Chauvin Pharmaceuticals Ltd., Surrey, UK) and phenylephrine 2.5% (Bausch & Lomb) eyedrops were instilled in both eyes for mydriasis and ocular lubricant (HPMC PAA gel; Alcon Laboratories) was applied to prevent corneal desiccation. Subcutaneous Hartmann's solution (2.5 mL/kg/h) and heat pads were provided at the end of the clinical assessment to assist recovery. Our clinical assessment protocol has been detailed previously.[27,28]

In the two animals (16_320, 16_321) with a passive electrode array, spectral-domain optical coherence tomography (SD-OCT; Spectralis; Heidelberg Engineering Gmbh, Heidelberg, Germany), color fundus photography (CFP; TRC-50DX mydriatic retinal camera; Topcon Medical Systems, Oakland, NJ, USA), and IOP (iCare Tonometer, Vantaa, Finland) were performed prior to surgery and at 2, 6, and 13 to 15 weeks postsurgery. Dark-adapted full-field electroretinography (ffERG; Espion E2; Diagnosys LLC, Lowell, MA, USA) was performed prior to surgery and at 13 to 15 weeks postsurgery. In the eight animals that received chronic electrical stimulation, SD-OCT, CFP, and IOP were performed prior to surgery, at 2 and 4 weeks postsurgery, and then every 4 weeks (±2 weeks) up to a maximum of 20 weeks postsurgery, while dark-adapted ffERG was performed prior to surgery and at 2 weeks postsurgery.

Electrode array insertion trauma to the retina was assessed from CFP and SD-OCT images and ffERG at 2 weeks postsurgery. Recording of the ffERG was performed after 20 minutes of dark adaptation in the implanted and fellow eyes simultaneously. The retinal response (mean of 5 measurements) was recorded for various light flash luminance levels (0.01–10 cd.s.m^{-2}), but just the combined rod–cone maximal ffERG response (10 cd.s.m^{-2}) is reported. The ratio (implanted: fellow eyes) of a-wave (photoreceptor component) and b-wave (post-receptoral component) amplitudes of the dark-adapted maximal ERG response (10 cd.s.m^{-2}) at 2 weeks was compared with baseline to confirm the global retinal function after surgery. IOP was averaged from five separate measurements and was used to ensure the normal recovery of pressure after surgery.

The long-term mechanical stability of the electrode array was assessed in both lateral and vertical (axial) planes. Lateral device movement was assessed from overlaid CFPs at each longitudinal time point using the optic disc diameter (DD) as the measuring unit. The edges of the electrode array are seen as a shadow in the ocular fundus and can be mapped relative to ocular features such as blood vessels. SD-OCT B-scans and matching infrared images were used to confirm the position of the implant if there was any doubt as to its position in the CFP. Axial implant stability was assessed from high-resolution volume and single-line SD-OCT B-scans overlying and adjacent to the electrode array and reported as electrode to retina (ER) distance (retinal pigment epithelium [RPE]/tapetum junction to inner electrode surface). Each B-scan was an average of 100 frames and follow-up mode was used longitudinally where possible. Separate B-scans were collected to align with the orientation of the columns and the rows of electrodes. The ER distance was measured from the center of each identified electrode, using the measuring tool within the Spectralis HEYEX software, as per our established protocol.[24,28] Due to field-of-view constraints, 10 to 30 electrodes from the total 46 were identified in each animal, so the tip and central-inferior sections of the array were adequately sampled. Arrays that were placed more temporally or superiorly had fewer electrodes imaged.

The long-term structural (from CFP and SD-OCT) and functional (from ffERG) status of the retina was evaluated in the two animals with passively implanted arrays for 13 to 15 weeks to give an indication of the long-term biocompatibility of the electrode array. The longitudinal clinical data was assessed in conjunction with histopathology data at the endpoint. CFPs and volumetric SD-OCT scans were assessed qualitatively by a clinician for any retinal pathology that might have developed between 2 weeks and endpoint. Retinal thickness (inner limiting membrane to RPE/tapetum junction) was measured at baseline, 2, and 13 to 15 weeks with SD-OCT at 10 evenly spaced regions at the electrode array tip, at the center of the array, adjacent to the array, and at the fellow eye area centralis, as per previously published methods.[28] This indicates whether there is any significant cell loss or retinal swelling over time. The a-wave amplitude ratio (13–15 weeks: baseline) from the dark-adapted ffERG (combined rod-cone maximal ERG response of 10 cd.s.m^{-2}) was used to assess for any changes in implanted eyes versus nonimplanted eyes and historic control eyes ($N = 23$).

Conformability of the electrode array was assessed qualitatively from SD-OCT images overlying the electrode array in conjunction with images from vertical histologic sections. The tissue at the edge of the electrode array was assessed for whether the tissue to implant transition was smooth or whether there was any damage or impact upon the retina, RPE/tapetum complex, and choroid structures. The angle subtended by the orientation of each disc electrode to the orientation of the overlying RPE/tapetum complex was measured with a protractor for tilt >10° as an indication of electrode array robustness. The number of electrodes with tilt was quantified relative to the total number of electrodes assessed. It was further noted whether there was any impact by electrodes or the silicone carrier upon the choroid/tapetum structures.

Termination, Dissection, and Histopathology Assessment

At the endpoint, animals were anesthetized for a separate acute electrophysiology experiment, killed, and the eyes gathered for histopathologic evaluation as described previously.[34] Each animal was overdosed with sodium pentobarbital i.v. (Leth-

Investigative Ophthalmology & Visual Science

Downloaded From: https://iovs.arvojournals.org/pdfaccess.ashx?url=/data/journals/iovs/936793/ on 03/19/2018

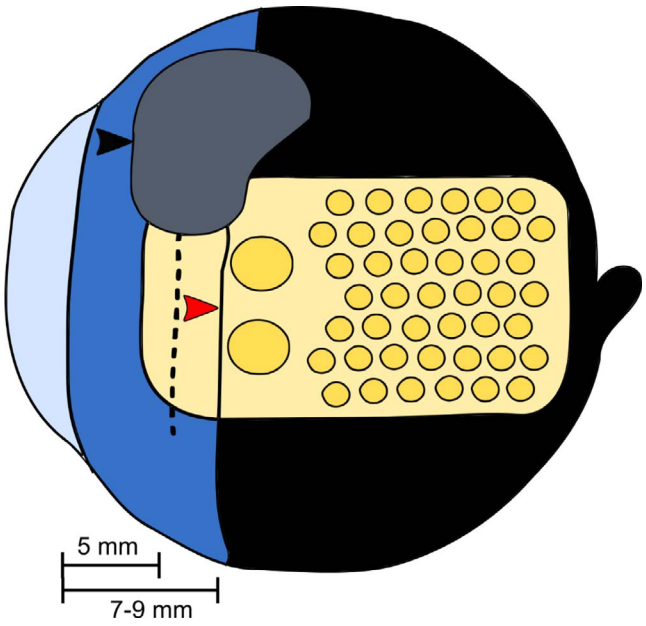

FIGURE 2. Schematic indicating position of scleral patch (*gray*), electrode array (*yellow*), and incision site (*dotted line*) relative to the limbus and the junction (*red arrowhead*) between thick anterior (*blue*) and thin posterior (*black*) sclera in feline eyes. The scleral incision was placed 5-mm posterior to the limbus and the thin posterior sclera begins 7- to 9-mm posterior to the limbus. The sclera under the patch (*black arrowhead*), at the incision site and overlying the electrode array (including the antero-posterior junction) was examined for any signs of fibrosis, infection, wound breakdown, and scleral erosion. Cornea is indicated in *light blue*, anterior (thick) sclera in *medium blue* and posterior (thin) sclera in *black*. Not to scale.

abarb; Virbac, New South Whales, Australia). Heparinized saline at 37°C was perfused via the left ventricle until venous outflow was clear, followed by perfusion with 0.8 to 1.2 L neutral buffered formalin (NBF) 10% at 4°C. The eyes were enucleated without cutting the lead-wire cable, and post-fixed in Davidson's modified fixative for 18 to 36 hours at room temperature, 50% ethanol for 6 to 8 hours at room temperature, before being stored in 70% ethanol at 4°C until dissection.

The sclera at the patch, incision site and overlying the electrode array was examined and photographed under a surgical microscope during dissection to assess the scleral patch position, the viability of patch sutures, and for any signs of fibrosis, infection, wound breakdown, and scleral erosion (Fig. 2). The electrode array was carefully removed from the eye after dyeing the electrode positions on the scleral tissue[28,34] and the array was examined to ensure that all electrodes were accounted for as part of an assessment of electrode robustness. Multiple full thickness strips of retina, choroid, and sclera were cut from the implanted and adjacent regions.[34] Tissue was embedded in agar and supported by foam inserts before transferring into 10% NBF for 1 to 3 hours, embedding in paraffin in a standard automated cycle, cutting vertical sections (5-µm thickness) with a microtome and staining with hematoxylin and eosin (H&E).[28,34] Micrographs were taken with an Axio Imager 2 upright microscope (Carl Zeiss AG) and Axiovision V4.8.2 software.

Histopathology grading as part of the biocompatibility assessment was performed using an established 4-level scoring system (from score 0: no observable difference to expected baseline, to score 4: a major variation from expected baseline) by two pathologists experienced in retinal pathology under random, double-blind conditions.[28] Data are presented for two passive implantation subjects (16_320 and 16_321) and compared with previously published data from two randomly selected historic control eyes.[28] Three histologic vertical sections were graded for each eye; a section oriented across the central width of the implant, and two parallel sections through the tip of the implant. The tissue surrounding the implant was assessed for scarring, fibroblastic response, acute and chronic inflammatory responses, and foreign body multinucleate giant cell response. The presence or absence of necrosis and retinal damage was noted, as was any damage away from the implant site. A randomized re-check performed in a subset of samples (10%) at 20-weeks postinitial evaluation verified internal scoring consistency. Because the data were consistent between scorers, the grades were averaged across scorers and the three sections located at the tip and central regions of the implant.

TABLE 2. Device Implantation Period and Testing Regime

Animal ID	Implant Period, wk	CFP, SD-OCT, IOP, wk Postsurgery	ffERG, wk Postsurgery	Histopathology Assessment
16_320	13	BL, 2, 6, 13	BL, 13	Y
16_321	15	BL, 2, 6, 15	BL, 15	Y
16_524	13	BL, 2, 4, 6, 13	BL, 2	N
16_525	20	BL, 2, 4, 13, 17, 20	BL, 2	N
16_526	20	BL, 2, 4, 10, 16, 20	BL, 2	N
16_527	9	BL, 2, 4	BL, 2	N
16_528	9	BL, 2, 4	BL, 2	N
16_530	15	BL, 2, 4, 8, 15	BL, 2	N
16_531	5	BL, 2, 5	BL, 2	N
17_532	12	2, 4, 8, 12	N	N

BL, baseline; Y, yes; N, no.

Statistical Analyses

The ffERG response amplitudes were analyzed with repeated-measures ANOVA and Bonferroni post hoc tests. Retinal thickness and ER distance were analyzed with Kruskal-Wallis and Dunn's post hoc tests for each animal. Statistical analyses were performed with a commercial software program (GraphPad Prism version 5; GraphPad Software Inc., La Jolla, CA, USA) using 5% significance.

RESULTS

Implantation Period

The mean (±SD) period of device implantation was 13.1 ± 4.7 weeks (Table 2). Seven animals successfully had the device implanted for the planned period of ≥12 weeks. Three animals were euthanized under veterinary and surgical advice (16_527, 16_528) or died unexpectedly (16_531) prior to the planned endpoint. Two animals (16_320, 16_321) had longitudinal clinical assessments (CFP, SD-OCT, and IOP) along with endpoint ffERG and histopathology assessment at 13 to 15 weeks (Table 2). The remaining eight animals had longitudinal clinical assessments plus ffERG at 2 weeks, but the endpoint retinal function and histopathology data will be assessed in a companion publication evaluating electrical stimulation safety.

Electrode Array Insertion Safety

The electrode array was inserted safely (with negligible to minor trauma only) in 80% (8/10) of animals. Seven animals

Investigative Ophthalmology & Visual Science

Downloaded From: https://iovs.arvojournals.org/pdfaccess.ashx?url=/data/journals/iovs/936793/ on 03/19/2018

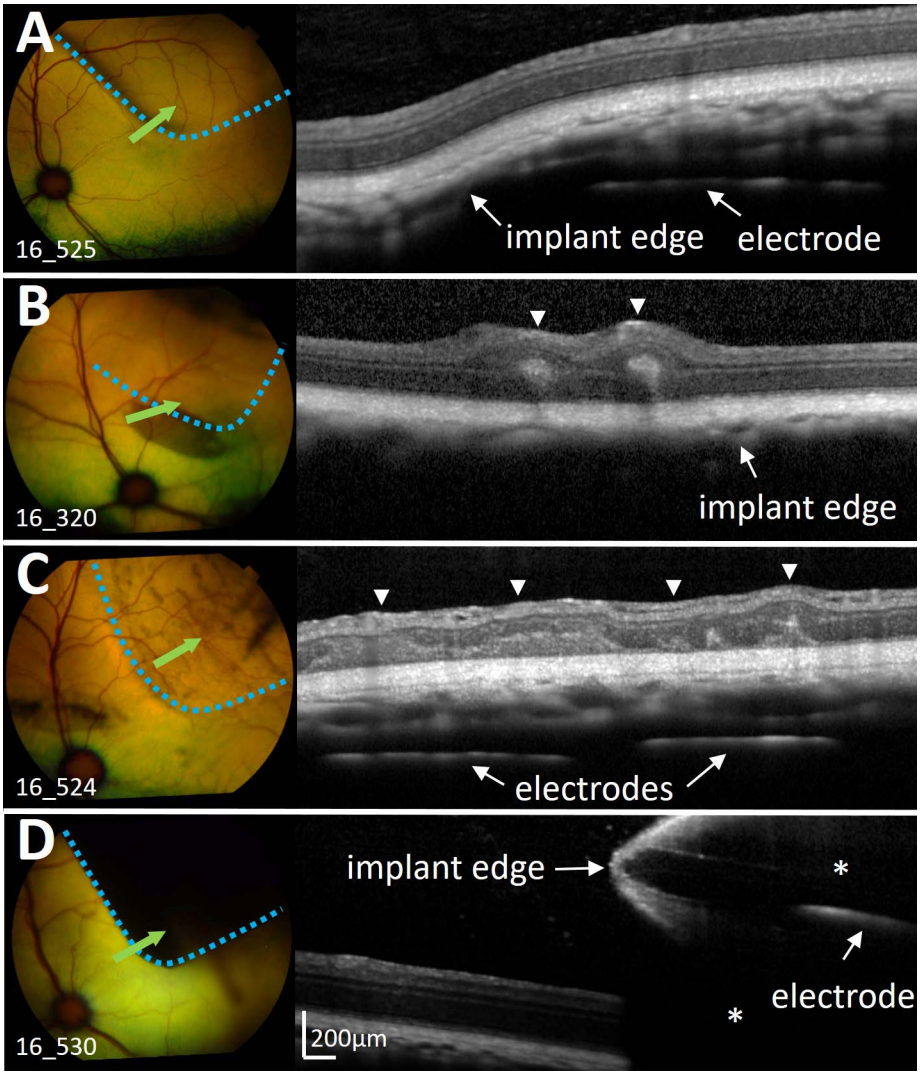

Figure 3. Electrode array insertion safety at 2 weeks postsurgery. (**A**) Representative example of a healthy implanted eye (16_525) with no retinal trauma following electrode array insertion (7/10 animals) shown by both CFP and SD-OCT. The outline of the electrode array (*blue dots*; implant edge) is seen as a shadow on the CFP. *Green arrow* indicates the position of the B-scan. (**B**) Implanted eye (16_320) with localized retinal change adjacent to the tip of the electrode array (1/10 animals), seen as two small retinal folds (*arrowheads* on SD-OCT) and hyperpigmentation on CFP. (**C**) Implanted eye (16_524) with extensive retinal changes overlying electrode array (1/10 animals), seen as multiple retinal folds (*arrowheads* on SD-OCT) and hyperpigmentation (on CFP) overlying the electrode array in lines perpendicular to the direction of array insertion. These changes occurred subsequent to a difficult insertion relating to choroidal bulging and subsequent buckling of the electrode array. (**D**) Implanted eye (16_530) with extensive retinal changes overlying electrode array (1/10 animals), due to a large suprachoroidal and subretinal hemorrhage (*) that formed due to a systemic bleeding disorder

had no retinal trauma following surgery (such as Fig. 3A), while one animal (16_320) had minor localized retinal trauma with two small retinal folds and hyperpigmentation at a small region adjacent to the tip (Fig. 3B) and also at the back portion of the electrode array. Importantly, the retina overlying the array was healthy. Two animals (16_524, 16_530) had extensive surgical trauma resulting in damage to the retina overlying the electrode array. Animal 16_524 developed multiple retinal folds and hyperpigmentation overlying the electrode array in lines perpendicular to the direction of array insertion (Fig. 3C). In this animal, the choroid bulged during surgery that made array insertion difficult and ultimately the array buckled, resulting in mechanical damage to the retina and pigment epithelium. On SD-OCT, predominantly the outer nuclear layer appears highly reflective and thickened, similar to retinal folds seen in another study.[35] There was no subretinal or suprachoroidal hemorrhage associated with these retinal changes during follow-up ophthalmic examinations by vitreoretinal surgeons. Histology sections (data not shown) depict folds within the outer nuclear layer, correlating with SD-OCT findings. Animal 16_530 had a large subretinal and suprachoroidal hemorrhage localized to the site of the electrode array (Fig. 3D), and was due to a systemic bleeding disorder in this animal that was subsequently diagnosed after surgery. Critically, there were no cases of vitreal hemorrhage or retinal detachment in any of the 10 animals. A summary of the results for each animal is shown in Table 3.

Individual ffERG traces are shown for each animal in the study illustrating both baseline and 2-week data in implanted and fellow eyes (Figs. 4A–G). Four animals showed consistent a- and b-wave amplitudes at both time points. The two animals (16_524 and 16_530) associated with major surgical complications exhibited a small reduction of amplitudes in the implanted eye at 2 weeks. Another animal (16_525) also had a

Investigative Ophthalmology & Visual Science

Downloaded From: https://iovs.arvojournals.org/pdfaccess.ashx?url=/data/journals/iovs/936793/ on 03/19/2018

Downloaded From: https://iovs.arvojournals.org/pdfaccess.ashx?url=/data/journals/iovs/936793/ on 03/19/2018

Table 3. Summary of Results

Animal ID	Surgical Complications	Lateral Movement	ER Distance	Dissection	Histopathology	Adverse Events
16_320	Mild localized retinal folds and hyperpigmentation adjacent to tip of array	Stable	Stable	Normal	Negligible to minor scarring, fibroblastic response, chronic inflammation. Minor to moderate acute inflammation and FBMNGC response	None
16_321	None	Stable	Stable	Normal	Negligible to minor scarring, fibroblastic response, chronic and acute inflammation, and FBMNGC response	None
16_524	Extensive retinal folds, hyperpigmentation overlying array	Stable	Major increase	Normal	Not applicable	None
16_525	None	Minor movement	Minor increase	Normal	Not applicable	None
16_526	None	Stable	Stable	Normal	Not applicable	None
16_527	None	Stable	Stable	Normal	Not applicable	Terminated early under veterinary and surgeon advice
16_528	None	Major movement	Stable	Fibrosis at scleral patch and wound breakdown at scleral incision	Not applicable	Terminated early under veterinary and surgeon advice
16_530	Major subretinal and suprachoroidal hemorrhage at array position	Stable	Not applicable	Normal	Not applicable	Systemic bleeding disorder
16_531	None	Major movement	Not applicable	Partial device extrusion through thick to thin scleral junction	Not applicable	Unexpected death prior to endpoint
17_532	None	Stable	Minor increase	Mild pus accumulation around scleral patch	Not applicable	Terminated early under veterinary and surgeon advice

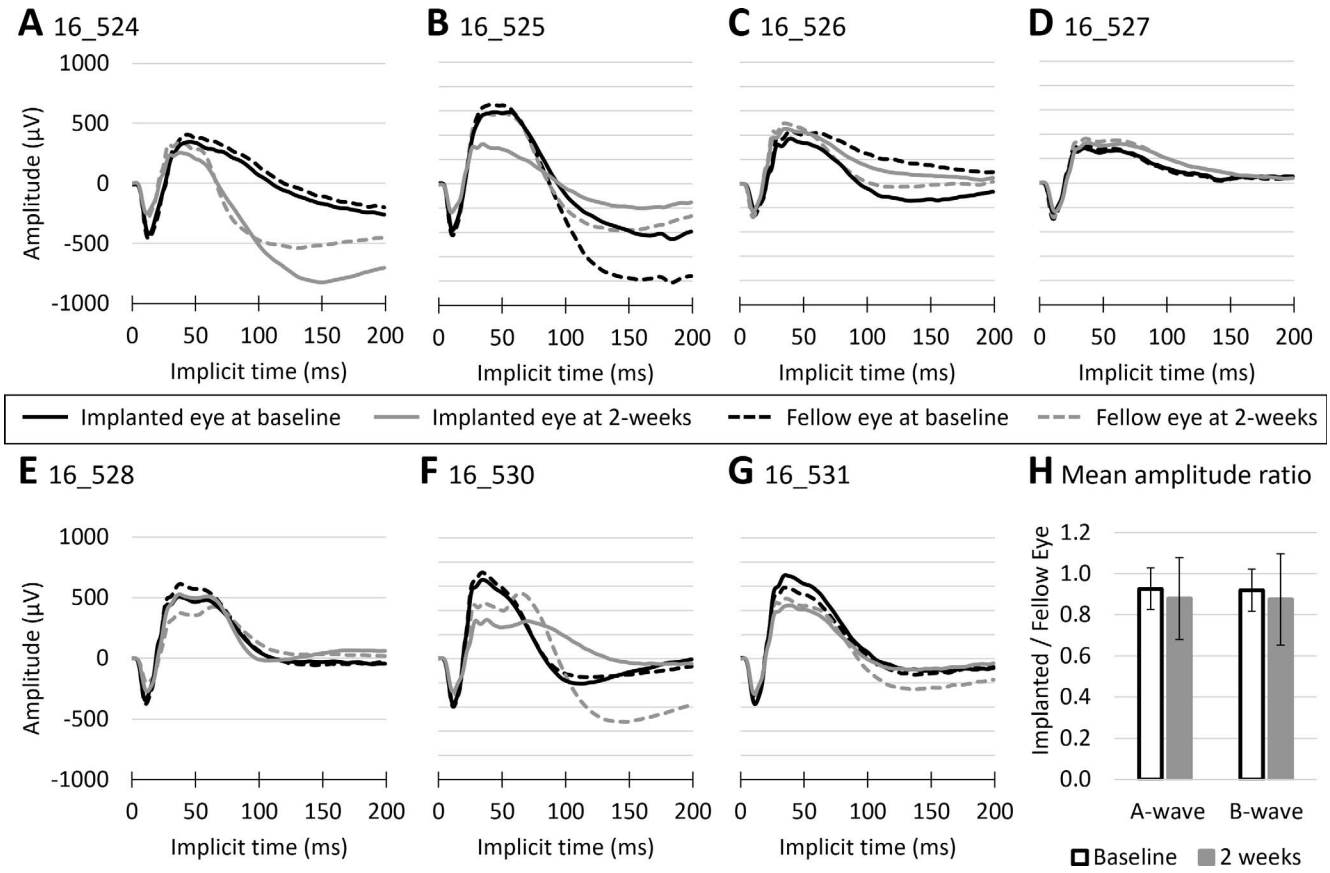

Figure 4. FfERG data at 2 weeks compared with baseline in implanted eyes and fellow eyes at 10 cd.s.m^{-2}. (**A–G**) Individual traces for each animal ($N = 7$ animals). (**H**) The mean ffERG response ratio (implanted: fellow eye) showed no significant difference between baseline and 2 weeks ($P > 0.05$, $N = 7$) for either the a-wave or b-wave amplitude (10 cd.s.m^{-2}). *Error bars*: 95% confidence interval.

mild reduction of a- and b-wave amplitudes in the implanted eye at 2 weeks. The a-wave and b-wave ffERG mean response ratio (implanted: fellow eye; 10 cd.s.m^{-2}) both showed no difference ($P > 0.05$, $N = 7$ animals) between baseline and 2 weeks, indicating normal global retinal function in implanted eyes after surgery across the group (Fig. 4H). IOP was found on average to be 1 to 3 mm Hg lower in the implanted eye relative to the fellow control eye at all postsurgery time points, but within clinically accepted levels (data not shown). Two animals experienced moderately raised IOP (16_321 = 25 mm Hg and 16_527 = 28 mm Hg) at 2 weeks postsurgery following the use of topical steroid, but IOP returned to baseline by 4 to 6 weeks so there was no risk of steroid-induced optic neuropathy.

Stability of Electrode Array

There was good mechanical stability of the electrode array in 80% (8/10) of animals over the monitoring period as determined from the amount of lateral movement (Fig. 5). Of these, seven showed some minimal movement during the 4-week initial settling period post surgery (≤1 DD; ~1.5 mm) and no movement over the remainder of the monitoring period (Fig. 5A). The other animal (16_525) had minor lateral movement (~1.75 DD, Fig. 5B) accompanied by a minor increase in ER distance (100 ± 32 μm, $P = 0.009$ Kruskal-Wallis, Fig. 6) at 12 weeks. Thereafter, there was no further lateral movement and the ER distance returned to baseline by 16 weeks. On dissection, these eight animals all had flat and well-encapsulated scleral patches with intact sutures and normal wound healing at the incision site.

There were two animals with major lateral implant movement of >3 DD over the implantation period (Fig. 5C). In one animal (16_528), lateral movement at 4 weeks coincided with an infection (abscess) that occurred at the temporal conjunctiva near to the scleral wound position. At dissection, thick fibrosis was evident under and around the scleral patch with signs that some of the sutures had pulled through the tissue due to wound breakdown at the scleral incision (Fig. 2). In the other animal (16_531), lateral movement at 4 weeks coincided with a diffusely bulged conjunctiva. At dissection, a partial extrusion of the implant through the junction of the thick to thin posterior sclera was seen, noting that the scleral incision and patch sutures were still intact (Fig. 2). These two animals were not the same two animals that had major surgical trauma. A summary of the results for each animal is shown in Table 3.

ER distance remained stable in five of the eight animals that could be followed over the monitoring period (Fig. 6). Of the three animals that showed an increase in ER distance, only one animal (16_524) had a major increase (451 ± 177 μm, $P < 0.0001$ Kruskal Wallis) over follow-up, which was likely related to the major surgical trauma from device buckling during insertion (Fig. 3C). The scleral patch and wound sites were intact on dissection. The other two animals showed a minor increase in ER distance of approximately 100 μm at 12 weeks (Fig. 6), and were not related to surgical trauma. One of these (16_525) had associated minor lateral movement but no complications on dissection, as discussed above. The other (17_532: 113 ± 22 μm, $P < 0.0001$ Kruskal Wallis) had an accompanying diffusely bulged conjunctiva at 12 weeks, and

Investigative Ophthalmology & Visual Science

Downloaded From: https://iovs.arvojournals.org/pdfaccess.ashx?url=/data/journals/iovs/936793/ on 03/19/2018

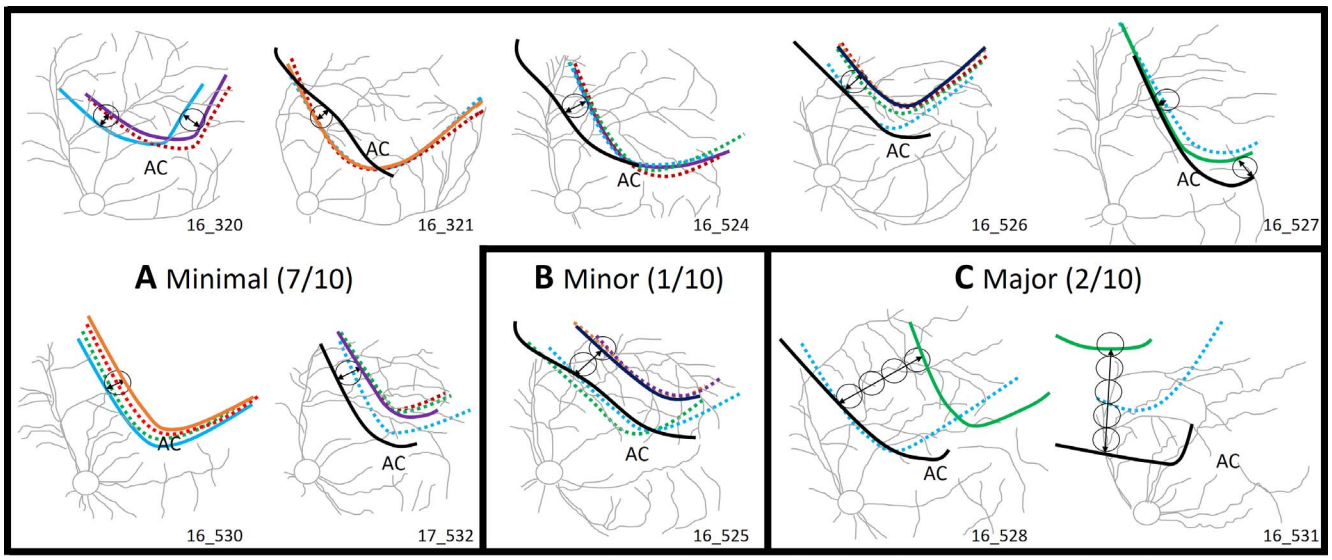

Figure 5. Lateral movement of the electrode array over the chronic implantation period. (**A**) Most animals (7/10) showed minimal movement of ≤1 DD over the monitoring period. (**B**) One animal (1/10) had minor movement of 1.75 DD at 12 weeks that subsequently stabilized. (**C**) Two animals (2/10) had major movement of >3 DD at 4 weeks. Note these were different animals to those with major surgical trauma. *Solid lines* indicate baseline and final time points and *dotted lines* indicate other time points as per color-coded legend. Two animals (16_320, 16_530) did not have a baseline CFP immediately after surgery due to poor visibility of the posterior segment.

reduced electrode visibility on SD-OCT, but no associated lateral movement (Fig. 5A). On dissection, the scleral wound, posterior sclera, and patch sutures were all intact, which correlates to the finding of minimal lateral movement. However, there was mild pus accumulation around and under the scleral patch (Fig. 2) indicating a localized infection and mild fibrous tissue down growth within the suprachoroidal pocket, both of which may account for the limited visibility of electrodes and the minor increase in ER distance. In the remaining two animals of the cohort, ER distance could not be determined due to (1) a significant hemorrhage over and under the electrode array from a systemic bleeding disorder (16_530), and (2) limited electrode visibility from major lateral movement (i.e., electrodes outside SD-OCT field of view; 16_531). A summary of the results for each animal is shown in Table 3.

Structural, Functional, and Histopathologic Evaluation of the Retina

The long-term structural, functional, and histopathologic status of the retina was evaluated in the two animals with passively implanted arrays for 13 to 15 weeks (Table 2; 16_320, 16_321). SD-OCT longitudinal scans, such as the representative images in Figure 7A, show no overt changes in the retinal lamination or health overlying and adjacent to the electrode array over the implanted period. In animal 16_320, there was a small increase in retinal thickness at the tip (~12 μm, $P < 0.05$) and a trend for increasing thickness overlying the array (~10 μm, $P > 0.05$) at 2 weeks, which both resolved by 13 weeks and likely indicates a mild inflammatory response (retinal edema) immediately postsurgery (Fig. 7B). This may be associated with the minor retinal trauma noted adjacent to the tip in this animal from surgery (Fig. 3B). There was no change in retinal

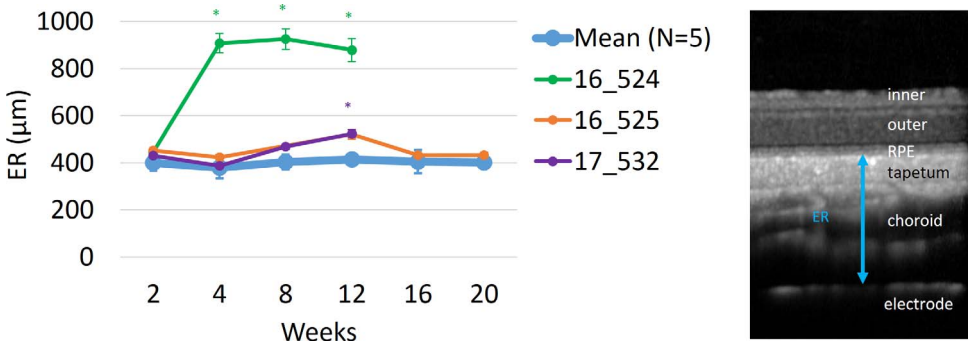

Figure 6. Axial stability of the electrode array over the chronic implantation period in eight animals. ER distance was measured from SD-OCT scans from the center of each electrode (*blue arrow*). Five animals showed no significant change in ER distance over time ($P > 0.05$, within each animal) with data shown as a mean ($N = 5$). One animal (16_524) showed a major increase in ER distance by 4 weeks, while two animals (16_525, 17_532) showed a minor increase in ER distance at 12 weeks. In 16_525, the increase in ER distance resolved by 16 weeks, but 17_532 was killed at 12 weeks so was not followed further. *Error bars*: mean of the animals with no change over time shown as 95% confidence interval of the normal range; individual animals shown as SEM. *Data points with significance of $P < 0.05$ on Dunn's multiple comparison post hoc test compared with 2 weeks.

Investigative Ophthalmology & Visual Science

Downloaded From: https://iovs.arvojournals.org/pdfaccess.ashx?url=/data/journals/iovs/936793/ on 03/19/2018

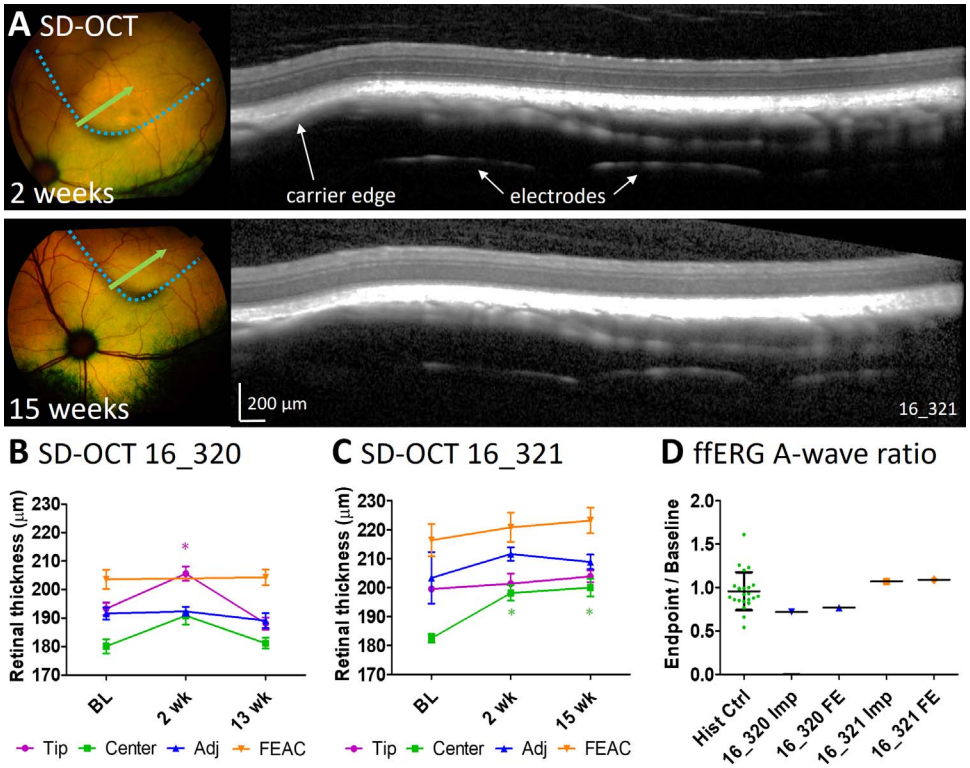

Figure 7. Evaluation of long-term retinal structure and function in the two animals with passively implanted electrode arrays (16_320, 16_321). (**A**) Representative SD-OCT (16_320) at 2 and 15 weeks. *Green arrow* indicates the follow-up scan position through the same section of retina at each time point. The retina remained well laminated and healthy over the implantation period. (**B**) In 16_320, there was a mild increase in retinal thickness at 2 weeks at the tip (*$P < 0.05$ Dunn's multiple comparison post hoc test relative to baseline) and a trend for increased thickness overlying the array center ($P > 0.05$), although it had resolved by 13 weeks. There was no change in retinal thickness in retina adjacent (Adj) to the array or at the fellow eye area centralis (FEAC) (all $P > 0.05$). (**C**) In 16_321, there was no change in retinal thickness between 2 and 15 weeks at any location. Baseline retinal thickness overlying the array was lower than at time points after implantation (*$P < 0.05$) because the implant was positioned superiorly to where the baseline scans were taken. (**D**) The a-wave amplitude ratio (endpoint/baseline) was equivalent in implanted (Imp) and fellow eyes (FE) within each animal and was within 1 SD (*error bars*) of the historic control data (Hist. Ctrl.; $N = 23$) for the flash intensity of 10 cd.s.m^{-2}.

thickness either adjacent to the array ($P > 0.5$) or at the fellow eye area centralis ($P > 0.05$). In animal 16_321, there was no change in retinal thickness ($P > 0.05$) between 2 and 15 weeks either at the tip of the array, overlying the array, adjacent to the array, or in the fellow control eye (Fig. 7C). However, baseline measurements were lower ($P < 0.05$) in the overlying array location relative to 2 and 15 weeks because the array location was superior to where the baseline measurements were taken. The baseline measurements for the other positions (tip, adjacent, fellow eye) were not statistically different from the later time points ($P > 0.05$). Photoreceptor function assessed with ffERG a-wave amplitude (10 cd.s.m^{-2}) for both animals showed the endpoint to baseline a-wave amplitude ratio for implanted and fellow control eyes to be equivalent and within 1 SD of the historic control sample data ($N = 23$ eyes of 23 animals; Fig. 7D).

In the two animals with passive implants histologic examination of vertical sections through the tip and central regions of the array show the location of the suprachoroidal pocket that held the electrode array (Fig. 8). There is a thin band of fibrous tissue that forms around the implant to encapsulate it (Fig. 8A'), consistent with our previous studies.[27,28] The retina overlying the electrode array position is healthy and well laminated in both animals with the passive implant (Figs. 8A, 8B). One animal (16_320) exhibited a small retinal fold adjacent to the electrode array tip (Fig. 8C), correlating with the 2-week SD-OCT findings of minor surgical trauma in Figure 3B. The fold is seen as a break within the inner and outer segments of the photoreceptors, and the overlying retina is folded upon itself. The photoreceptor somas are sparser at the folded region than neighboring tissue and the outer plexiform and inner nuclear layers have thinned.

Histopathologically, both animals exhibited negligible to minor variations from the expected baseline (grade 0–1) for scarring, fibroblastic response, and chronic inflammation (Fig. 9; Table 3). For acute inflammation and foreign body multinucleate giant cell responses, one animal (16_321) scored negligible to minor variations from expected baseline (grade 0–1), while the other animal with the minor retinal trauma adjacent to the electrode array tip (16_320) scored minor to moderate variations (grade 1–2). In each animal, the three histology sections from different retinal locations had similar histopathology grading. It should be particularly noted in 16_320, where there was retinal trauma at the tip of the array as a result of the surgery, the inflammatory response was not simply localized to the histologic section that went through the localized region of trauma. The nonimplanted historic controls had negligible variations from expected baseline for all types of tissue response (grade 0).[28] There were no necrosis or retinal damage noted at the tip or central regions overlying the implant, except for a small retinal fold adjacent to the tip in one animal (16_320; Fig. 8C), correlating with the in vivo SD-OCT findings of a small fold and hyperpigmentation (Fig. 3B). Overall, the tissue response at 13 to 15 weeks of implantation is consistent with a mild foreign body reaction.[27,36] Together, the ffERG, SD-OCT, histology, and histopathology results

Investigative Ophthalmology & Visual Science

Downloaded From: https://iovs.arvojournals.org/pdfaccess.ashx?url=/data/journals/iovs/936793/ on 03/19/2018

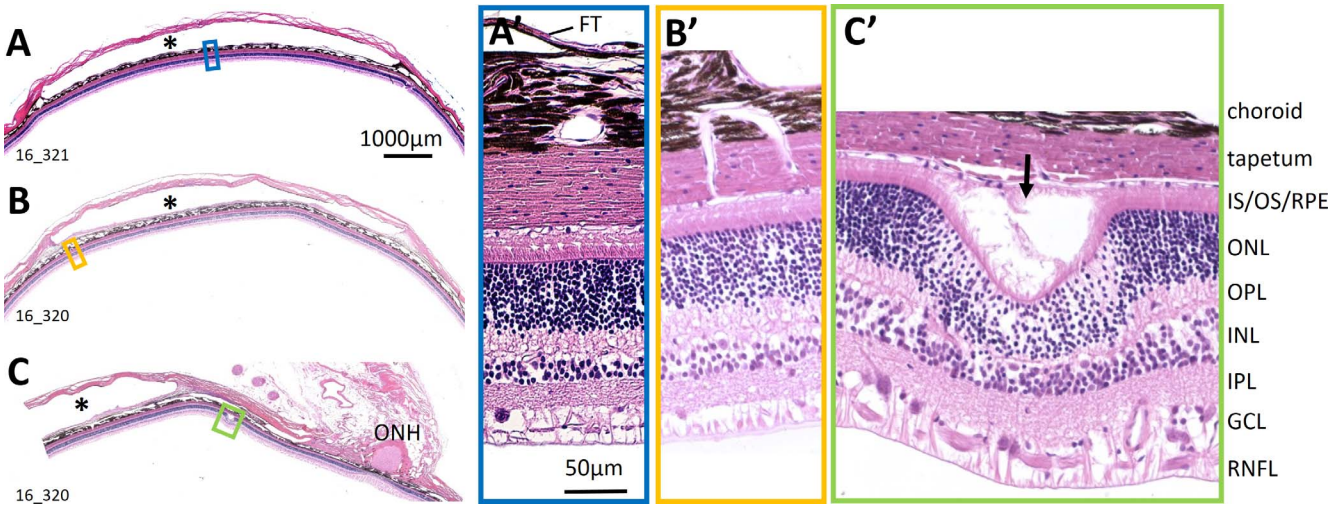

Figure 8. Histology. (**A**) Representative mosaic (×2.5) through the central suprachoroidal pocket of 16_321. The electrode array position in the suprachoroidal pocket (*) is conformable to the sclera and retina/tapetum/choroid. (**A'**) The *blue box* region from (**A**) at higher power (×20) shows a healthy retina overlying the electrode array with a thin layer of fibrous tissue on the edge of the pocket, as expected.[27,28] (**B**) Representative mosaic (×2.5) through the central suprachoroidal pocket of 16_320. (**B'**) The *yellow box* region from (**B**) at higher power (×20) shows a healthy retina overlying the electrode array. (**C**) Mosaic (×2.5) through the edge of the suprachoroidal pocket and adjacent retina and the optic disc of 16_320. (**C'**) The *green box* region from (**C**) at higher power (×20) shows a small retinal fold (*arrow*) and associated RPE changes adjacent to the electrode array that occurred during surgery and correlates to the SD-OCT findings shown in Figure 3B. ONH, optic nerve head; FT, fibrous tissue; IS/OS/RPE, inner segments of photoreceptors/outer segments/retinal pigment epithelium; ONL, outer nuclear layer; OPL, outer plexiform layer; INL, inner nuclear layer; IPL, inner plexiform layer; GCL, ganglion cell layer; RNFL, retinal nerve fiber layer. *Scale bar* in (**A**) applies (**A**–**C**). *Scale bar* in (**A'**) applies (**A'**–**C'**).

indicate the implant is biocompatible with the retinal tissue over the 13 to 15 weeks of chronic passive implantation, with minimal effects on retinal structure, function, and foreign body tissue response.

Electrode Array Conformability and Electrode Robustness

SD-OCT volume scans showed conformability of the array to the retinal curvature, with a smooth interface between the array and the choroid (Fig. 10A). The SD-OCT data are supported by the histology data (Fig. 8), which also show conformability between the edge of the suprachoroidal pocket and the adjacent choroid and sclera. In two animals (16_525 and 16_526) at a single corner tip electrode (superiorly and inferiorly, respectively), there was minor edge pressure on the choroid/tapetum from the silicone carrier and electrode, but no effect on the overlying retina (Fig. 10B). These electrodes only had tilts of 5° relative to the curvature of the overlying RPE/tapetum boundary, but were able to impact the choroid due to their position as a corner electrode. A third electrode (from 16_26 middle of array) also had a mild impact (pressure) on the choroid, due to tilt development over time of 17°. Hence, from 139 electrodes examined in total, only three (2%) had pressure on the choroid, and the pressure was very minor/localized and unlikely to affect the choroidal blood supply to the retina. Individual electrodes were found to be robust in vivo, with only the one electrode (0.7%) showing >10° tilt relative to the curvature of the overlying RPE/tapetum boundary. It is possible this electrode tilted over time due to development of fibrosis under the electrode. Additionally, when the electrode arrays were removed at dissection, no electrodes had detached from the silicone carrier, indicating the electrodes were stable and robust over the chronic implantation period.

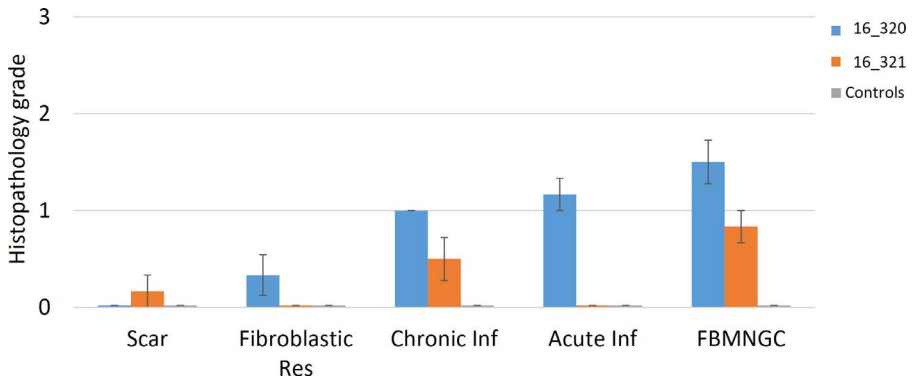

Figure 9. Histopathology grading as a mean score from two pathologists on a 4-point scale (see Methods). Three sections from the tip and central regions overlying the final array position were graded after 13 to 15 weeks of implantation and had acceptable levels of tissue response. Historic nonimplanted controls showed zero tissue response. *Error bars*: SEM. Res, response; Inf, inflammation; FBMNGC, foreign body multinucleate giant cell response.

Investigative Ophthalmology & Visual Science

Downloaded From: https://iovs.arvojournals.org/pdfaccess.ashx?url=/data/journals/iovs/936793/ on 03/19/2018

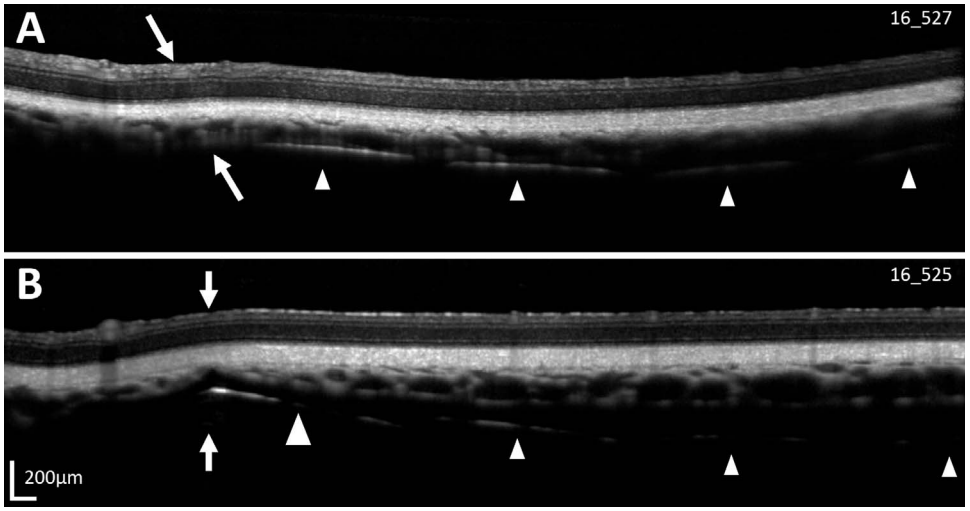

FIGURE 10. Electrode array conformability and electrode robustness. (**A**) Representative SD-OCT scan (16_527) showing the smooth interface between the array and the choroid/sclera (*arrows*) that occurs in most (8/10) animals. Electrodes (*arrowheads*) are parallel to the RPE/tapetum complex. (**B**) Representative SD-OCT scan (16_525) showing a minor local edge pressure on the choroid/tapetum (*arrows*) from the silicone carrier and an electrode at the corner of the electrode array tip as occurred in two animals. This electrode (*large arrowhead*) had a mild 5° tilt relative to the RPE/tapetum orientation. This edge pressure only occurred at a single corner electrode in both cases and did not impact the retina.

DISCUSSION

This chronic preclinical study found that the 44-channel suprachoroidal electrode array has an acceptable passive safety profile to proceed to clinical trial. Eight of 10 animals had excellent electrode array insertion safety, with seven having no damage at all to the retina and one with only small, localized retinal folds and hyperpigmentation adjacent to the electrode array tip. The passive chronic preclinical study conducted previously with our prototype array[27] found that small subretinal hematomas developed in all seven eyes within 2-weeks postoperatively, and resolved into hyperpigmentary lesions on CFP over time, and in one animal there was an overt subretinal hemorrhage that caused extended elevation of the retina, taking 7 weeks to resolve. Furthermore, the ffERG b-wave amplitude in those animals increased in implanted eyes at 2 weeks postoperatively, which was thought to be linked to mild retinal edema.[27] Interestingly, the current 44-channel study, did not have any occurrences of subretinal hematomas or hemorrhages aside from the one animal (16_530) that developed a combined subretinal and suprachoroidal hemorrhage and was later diagnosed as having a systemic bleeding disorder. The current study also did not show any increase in either the a-wave or b-wave ffERG amplitude at 2 weeks compared with the fellow eye or the baseline, although the single animal with the localized folds and hyperpigmentation adjacent to the electrode array did have mild retinal swelling overlying the tip and center of the array on retinal thickness measurements. Our previous chronic electrical stimulation study with a prototype array[28] also found some cases of hyperpigmentation near the tip of the electrode array similar to that found in the one animal with localized retinal folds and hyperpigmentation in the current study. Hence, there were fewer occurrences of minor trauma at the tip of the electrode array with the 44-channel array compared with the prototype arrays[27,32] indicating an improved surgical outcome with the current design.

Because the same surgeons implanted the electrode arrays in both our previous studies and the current study, it is possible there is a mild learning effect contributing to the improved surgical outcome associated with the evaluation of the current electrode array. However, any learning effect is likely to be small given the surgeons have now performed over 200 preclinical surgeries across multiple studies. In the previous prototype passive study it is likely the retinal damage near the array tip was due to the use of electrode arrays of 19 mm in length (the current study and the previous chronic stimulation study both used 17-mm long arrays). This reduction was in response to our previous observation that in a feline eye a 19-mm electrode array induces retinal damage near the array tip due to its close proximity to the optic disc and the insertion point of the short posterior ciliary arteries.[32] However, the two major surgical complications in this study (extensive retinal folds following array buckling with difficult insertion following choroidal bulging, and subretinal and suprachoroidal hemorrhage linked to a bleeding disorder) did not occur in the previous studies, although choroidal bulging itself has been a common issue reported in the surgical notes across all three preclinical studies.

In considering surgical implantation safety, it is interesting that all three patients with the prototype suprachoroidal retinal prosthesis developed a combined subretinal and suprachoroidal hemorrhage at 3 to 4 days postoperatively that subsequently resolved.[24] Animals in the current 44-channel preclinical study did not show any retinal hemorrhage postoperatively aside from the animal with the systemic bleeding disorder, but given it occurred in the previous patient trial, there is a likelihood that it could occur again in human surgery. It should also be noted that there was no explicit outer retinal damage in the current preclinical study from electrode array insertion. The epiretinal and subretinal approaches carry a higher inherent risk of retinal damage because the implant makes direct contact with the retina. There are reports of localized photoreceptor loss/disruption overlying subretinal implants[37–39] and localized retinal damage and/or gliosis from tacking or contact pressure with epiretinal implantation.[40,41] Hence, the surgical complications noted in the current study are not as severe as some of the complications recognized by other surgical approaches.

This study showed that eight of 10 animals exhibited excellent mechanical stability of the implant over time with $\leq$2 DD of lateral movement. Our previous passive chronic study with a prototype electrode array showed lateral movement of $\leq$3 DD in six animals, noting that only four had 3-months

Investigative Ophthalmology & Visual Science

Downloaded From: https://iovs.arvojournals.org/pdfaccess.ashx?url=/data/journals/iovs/936793/ on 03/19/2018

implantation, while the other two animals could only be followed for 2 weeks.[27] One of the animals that was only followed for 2 weeks was later found to have its implant extruding from the sclera, so it is possible that it may have had greater movement if CFP results were able to have been obtained at 3 months.[27] Additionally, our previous chronic active electrical stimulation study with a prototype electrode array[28] showed lateral movement of $\leq$2 DD in all seven animals over 15-weeks implantation and our prototype clinical trial[24] showed no lateral movement nor signs of extrusion. Hence, our current study with the 44-channel array showed similar mechanical stability to the previous preclinical prototype studies, with the exception of the two animals with >3 DD lateral movement; one due to an infection causing scleral wound breakdown and the other due to partial electrode array extrusion. The implant extrusion noted in the previous prototype passive study was thought to be due to a different angle of the leadwire cable at rest with respect to the implant body plane (27° compared with 0°–13° for the other animals).[27] Whereas in the current study, the partial array extrusion (16_531) occurred due to erosion of the sclera at the junction of the thick to thin sclera, while the scleral incision site remained intact. Speculatively, there may be localized increased mechanical stiffness of the 44-channel array at the location of the thick to thin scleral junction compared with the previous prototype arrays, because the orientation of the return electrodes has rotated 90° and they are located close to this junction (see Fig. 2). However, the local stiffness at this region could not be quantified or assessed, and in the other nine animals scleral erosion did not occur.

The long-term retinal structure and function was maintained over time and histopathology showed a mild foreign body response to chronic implantation (fibrosis grade 0–1; inflammation grade 0–1.5), as is typical for silicone implants.[36] These results are comparable to those from our prototype preclinical passive chronic safety study,[27] which found retinal structure and function was maintained from 2-weeks to 3-months implantation and the presence of a mild (grade 1) chronic inflammatory response and mild fibrosis in implanted eyes on histopathology. The previous chronic electrical stimulation preclinical prototype study[28] also found the electrode array to be well tolerated during 3-months chronic implantation (no change to retinal structure or function) with a minimal foreign body response (grade 0–1) and no adverse clinical or histologic findings aside from that due to implantation surgery. It is noteworthy that the prototype suprachoroidal clinical trial results showed the electrode to retina distance increased in all patients over 12 months.[24] This may possibly represent a stimulus-induced fibrotic and/or inflammatory response in the suprachoroidal pocket. Furthermore, two of three patients implanted with an intrascleral prosthesis developed stimulation-induced iridocyclitis within the first 6 months of surgery, which likely occurred due to inflammation at the pars plana where the return electrode was situated.[15] Iridocyclitis was not observed in either the suprachoroidal clinical trial,[24] or any of the suprachoroidal preclinical studies[27,28] including the current study. Further studies are required to clarify the stimulus limits for suprachoroidal stimulation.

The electrode array conformability to the retinal curvature and electrode robustness was excellent in the current study, with a smooth electrode array to tissue interface and electrodes remaining intact upon array removal at dissection. Therefore, despite changes in the mechanical properties within both the electrode array and the leadwire cable, the suprachoroidal array has maintained excellent conformability and robustness. The prototype clinical trial also exhibited smooth conformability of the array to the retinal curvature on SD-OCT imaging and all electrodes remained functional over the 24 months of the trial.

Despite the generally positive results in the current study, there were four animals (16_524, 16_528, 16_530, 16_531) that had significant surgical or electrode stability complications. The feline model was selected as it has a similar axial length, retinal structure, and retinal function to humans; however, there are important anatomic differences that account for the complications observed in feline, and therefore it is unlikely they will occur in human. First, from our experience, the feline choroid is prone to bulging during surgery, making insertion of a suprachoroidal electrode array difficult and increasing the risk of the electrode array buckling and causing retinal damage (i.e., 16_524). Human surgery is performed in patients with retinal degeneration and severely atrophic choroids, greatly reducing this risk. No evidence of choroidal bulging was observed in our clinical trial. Second, it is not feasible to screen for systemic bleeding disorders in cats (i.e., 16_530); however, a bleeding disorder in humans would be known prior to surgery. Third, feline sclera comprises a 7- to 9-mm thick anterior band, and is very thin posteriorly, whereas human sclera is thicker and more uniform.[42] The thin posterior feline sclera increases the risk of posterior scleral erosion and subsequent electrode array extrusion (i.e., 16_531). It also dictates that the scleral incision must be placed anteriorly within the thick component for wound stability in felines, however, an anterior incision is more exposed, and therefore more prone to infection (i.e., 16_528) than in human surgery[33] where a more posterior incision is protected by the lateral rectus. Hence, we are confident the differences in feline eye anatomy and surgical procedures make it more susceptible to the complications we observed, and therefore we expect the 44-channel suprachoroidal array to have an improved safety record as we move to clinical trials.

The strengths of this study include chronic implantation period of the final 44-channel electrode array design in a greater number of animals than assessed previously in preclinical studies with our prototype array and the ability to directly compare the surgical, mechanical stability, and histopathology results with the previous prototype safety studies in the feline model. The limitations of this study include the use of an animal model that requires a more anterior scleral incision and has thin posterior sclera, so there are seemingly higher risks of surgical and stability complications than in human. We also had three animals that did not complete the planned full 12 weeks of implantation due to complications. Furthermore, we only assessed endpoint retinal structure and function and histopathology outcomes in the two purely passively implanted animals in the interests of the best use of animal resources. The other eight animals were rolled into an active electrical stimulation study, and thus the histology results will be published in a companion manuscript.

Development of the 44-channel suprachoroidal electrode array was performed in conjunction with the perspectives and feedback from the patients who used the first in-human prototype device in the clinical trial of a suprachoroidal retinal prosthesis, and as such, we have increased the field of view and the number of electrodes to enrich the visual experience. The wide field of view possible with a suprachoroidal device is one of the advantages of the suprachoroidal location (along with a simple surgery, good device stability, and low risk of SAEs) and has potential for improving navigational outcomes and quality of life in patients. The results from the present study indicate that the change in mechanical characteristics from the prototype electrode arrays to the current 44-channel electrode array do not pose any increased safety risks than that already known prior to proceeding to human trial. These

Downloaded From: https://iovs.arvojournals.org/pdfaccess.ashx?url=/data/journals/iovs/936793/ on 03/19/2018

results will be paired with a companion publication evaluating the safety of chronic electrical stimulation using the 44-channel electrode array in our preclinical model.

In summary, the 44-channel suprachoroidal retinal prosthesis has an acceptable safety profile to proceed to clinical trial, with 80% of animals demonstrating safe surgical implantation and 80% demonstrating excellent implant stability (60% with both surgical safety and array stability). Biocompatibility of the electrode array was excellent with normal retinal structure and function and only a minor foreign body response evident after 13 to 15 weeks of chronic implantation. We expect that the safety profile will improve in the clinical setting as the complications relating to (1) a bulged choroid in surgery, (2) a systemic bleeding disorder, (3) an infection at the incision site, and (4) a thin posterior sclera, are specific to the feline model.

Acknowledgments

The authors thank the following people for their respective contributions: Vanessa Maxim and Tara Lofhelm (Bionics Institute) for device fabrication, Tamara Brawn (Bionic Vision Australia, BVA) and BVA staff for administrative support, Fenella Long and Sue Peirce (St. Vincent's Hospital Melbourne) for veterinary advice, and the staff of the Biological Research Centre (University of Melbourne) and the Experimental Medical and Surgical Research Unit (St. Vincent's Hospital Melbourne) for support with animal care.

Supported by the ARC Special Research Initiative in Bionic Vision Science and Technology grant to Bionic Vision Australia (RKS; Canberra, ACT, Australia); National Health and Medical Research Council (NHMRC) Grant 1082358 (PJA; Canberra, ACT, Australia); NHMRC Grant 1063093 (MNS). The Bionics Institute and the Centre for Eye Research Australia wish to acknowledge the support of the Victorian Government through its Operational Infrastructure Support Program (VIC, Australia).

Disclosure: **C.J. Abbott**, None; **D.A.X. Nayagam**, P; **C.D. Luu**, None; **S.B. Epp**, None; **R.A. Williams**, None; **C.M. Salinas-LaRosa**, None; **J. Villalobos**, P; **C. McGowan**, None; **M.N. Shivdasani**, P; **O. Burns**, P; **J. Leavens**, Cochlear Ltd (E); **J. Yeoh**, None; **A.A. Brandli**, None; **P.C. Thien**, None; **J. Zhou**, None; **H. Feng**, None; **C.E. Williams**, P; **R.K. Shepherd**, None; **P.J. Allen**, P

References

1. Shepherd RK, Shivdasani MN, Nayagam DA, Williams CE, Blamey PJ. Visual prostheses for the blind. *Trends Biotechnol*. 2013;31:562–571.
2. Bareket L, Barriga-Rivera A, Zapf MP, Lovell NH, Suaning GJ. Progress in artificial vision through suprachoroidal retinal implants. *J Neural Eng*. 2017;14:045002.
3. Brandli A, Luu CD, Guymer RH, Ayton LN. Progress in the clinical development and utilization of vision prostheses: an update. *Eye Brain*. 2016;8:15–25.
4. Lewis PM, Ayton LN, Guymer RH, et al. Advances in implantable bionic devices for blindness: a review. *ANZ J Surg*. 2016;86:654–659.
5. Liew G, Michaelides M, Bunce C. A comparison of the causes of blindness certifications in England and Wales in working age adults (16–64 years), 1999–2000 with 2009–2010. *BMJ Open*. 2014;4:e004015.
6. Luo YH-L, da Cruz L. The Argus® II retinal prosthesis system. *Prog Retin Eye Res*. 2016;50:89–107.
7. Stingl K, Bartz-Schmidt KU, Besch D, et al. Subretinal visual implant alpha IMS–clinical trial interim report. *Vis Res*. 2015;111:149–160.
8. Hornig R, Dapper M, Le Joliff E, et al. Pixium vision: first clinical results and innnovative developments. In: Gabel V, ed. *Artificial Vision*. Cham, Switzerland: Springer; 2017:99–113.
9. Keserü M, Feucht M, Bornfeld N, et al. Acute electrical stimulation of the human retina with an epiretinal electrode array. *Acta Ophthalmol*. 2012;90:e1–e8.
10. Klauke S, Goertz M, Rein S, et al. Stimulation with a wireless intraocular epiretinal implant elicits visual percepts in blind humans. *Invest Ophthalmol Vis Sci*. 2011;52:449–455.
11. Lorach H, Goetz G, Mandel Y, et al. Performance of photovoltaic arrays in-vivo and characteristics of prosthetic vision in animals with retinal degeneration. *Vis Res*. 2015;111:142–148.
12. Rizzo JF III. Update on retinal prosthetic research: the Boston Retinal Implant Project. *J Neuroophthalmol*. 2011;31:160–168.
13. Chow AY, Bittner AK, Pardue MT. The artificial silicon retina in retinitis pigmentosa patients (an American Ophthalmological Association thesis). *Trans Am Ophthalmol Soc*. 2010;108:120–154.
14. Lee S, Ahn JH, Seo J-M, Chung H, Cho D-I. Electrical characterization of 3D Au microelectrodes for use in retinal prostheses. *Sensors*. 2015;15:14345–14355.
15. Fujikado T, Kamei M, Sakaguchi H, et al. One-year outcome of 49-channel suprachoroidal–transretinal stimulation prosthesis in patients with advanced retinitis pigmentosa. *Invest Ophthalmol Vis Sci*. 2016;57:6147–6157.
16. Suaning G, Lovell N, Lehmann T. Neuromodulation of the retina from the suprachoroidal space: the Phoenix 99 implant. Paper presented at: Biomedical Circuits and Systems Conference (BioCAS); October 22–24, 2014; Lausanne, Switzerland.
17. Stingl K, Zrenner E. Electronic approaches to restitute vision in patients with neurodegenerative diseases of the retina. *Ophthalmic Res*. 2013;50:215–220.
18. Humayun MS, Dorn JD, Da Cruz L, et al. Interim results from the international trial of Second Sight's visual prosthesis. *Ophthalmology*. 2012;119:779–788.
19. da Cruz L, Dorn JD, Humayun MS, et al. Five-year safety and performance results from the Argus II retinal prosthesis system clinical trial. *Ophthalmology*. 2016;123:2248–2254.
20. Rizzo S, Belting C, Cinelli L, et al. The Argus II Retinal Prosthesis: 12-month outcomes from a single-study center. *Am J Ophthalmol*. 2014;157:1282–1290.
21. Mills J, Jalil A, Stanga P. Electronic retinal implants and artificial vision: journey and present. *Eye*. 2017;31:1383–1398.
22. Kitiratschky VB, Stingl K, Wilhelm B, et al. Safety evaluation of "retina implant alpha IMS"—a prospective clinical trial. *Graefes Arch Clin Exp Ophthalmol*. 2015;253:381–387.
23. Stingl K, Gekeler F, Bartz-Schmidt KU, et al. Fluorescein angiographic findings in eyes of patients with a subretinal electronic implant. *Curr Eye Res*. 2013;38:588–596.
24. Ayton LN, Blamey PJ, Guymer RH, et al. First-in-human trial of a novel suprachoroidal retinal prosthesis. *PLoS One*. 2014;9:e115239.
25. Shivdasani MN, Sinclair NC, Dimitrov PN, et al. Factors affecting perceptual thresholds in a suprachoroidal retinal prosthesisfactors affecting retinal prosthesis thresholds. *Invest Ophthalmol Vis Sci*. 2014;55:6467–6481.
26. Sinclair NC, Shivdasani MN, Perera T, et al. The appearance of phosphenes elicited using a suprachoroidal retinal prosthesisphosphenes of a suprachoroidal retinal prosthesis. *Invest Ophthalmol Vis Sci*. 2016;57:4948–4961.
27. Villalobos J, Nayagam DA, Allen PJ, et al. A wide-field suprachoroidal retinal prosthesis is stable and well tolerated

Downloaded From: https://iovs.arvojournals.org/pdfaccess.ashx?url=/data/journals/iovs/936793/ on 03/19/2018

following chronic implantation. *Invest Ophthalmol Vis Sci*. 2013;54:3751–3762.

28. Nayagam DAX, Williams RA, Allen PJ, et al. Chronic electrical stimulation with a suprachoroidal retinal prosthesis: a preclinical safety and efficacy study. *PLoS One*. 2014;9: e97182.
29. Bertschinger DR, Beknazar E, Simonutti M, et al. A review of in vivo animal studies in retinal prosthesis research. *Graefes Arch Clin Exp Ophthalmol*. 2008;246:1505–1517.
30. Merrill DR, Bikson M, Jefferys JG. Electrical stimulation of excitable tissue: design of efficacious and safe protocols. *J Neurosci Methods*. 2005;141:171–198.
31. Thien PC, Millard R, Epp SB, Nayagam DA. A flexible wireless system for preclinical evaluation of a retinal prosthesis. *Sensor Mater*. 2018;30:269–286.
32. Villalobos J, Allen PJ, McCombe MF, et al. Development of a surgical approach for a wide-view suprachoroidal retinal prosthesis: evaluation of implantation trauma. *Graefes Arch. Clin Exp*. 2012;250:399–407.
33. Saunders AL, Williams CE, Heriot W, et al. Development of a surgical procedure for implantation of a prototype suprachoroidal retinal prosthesis. *Clin Exp Ophthalmol*. 2014;42:665–674.
34. Nayagam DA, McGowan C, Villalobos J, et al. Techniques for processing eyes implanted with a retinal prosthesis for localized histopathological analysis. *J Vis Exp*. 2013;78:50411.
35. Chen J, Qian H, Horai R, Chan C-C, Caspi RR. Use of optical coherence tomography and electroretinography to evaluate retinal pathology in a mouse model of autoimmune uveitis. *PLoS One*. 2013;8:e63904.
36. Vistnes LM, Ksander GA, Kosek J. Study of encapsulation of silicone rubber implants in animals: a foreign body reaction. *Plast Reconstr Surg*. 1978;62:580–588.
37. Chow AY, Pardue MT, Chow VY, et al. Implantation of silicon chip microphotodiode arrays into the cat subretinal space. *IEEE Trans Neural Syst*. 2001;9:86–95.
38. Montezuma SR, Loewenstein J, Scholz C, Rizzo JF. Biocompatibility of materials implanted into the subretinal space of Yucatan pigs. *Invest Ophthalmol Vis Sci*. 2006;47:3514–3522.
39. Yu W, Wang X, Zhao C, et al. Biocompatibility of subretinal parylene-based Ti/Pt microelectrode array in rabbit for further artificial vision studies. *J Ocul Biol Dis Infor*. 2009;2:33–36.
40. Güven D, Weiland JD, Fujii G, et al. Long-term stimulation by active epiretinal implants in normal and RCD1 dogs. *J Neural Eng*. 2005;2:S65.
41. Roessler G, Laube T, Brockmann C, et al. Angiographic findings following tack fixation of a wireless epiretinal retina implant device in blind RP patients. *Graefes Arch Clin Exp Ophthalmol*. 2011;249:1281–1286.
42. Olsen TW, Aaberg SY, Geroski DH, Edelhauser HF. Human sclera: thickness and surface area. *Am J Ophthalmol*. 1998; 125:237–241.

Investigative Ophthalmology & Visual Science

Downloaded From: https://iovs.arvojournals.org/pdfaccess.ashx?url=/data/journals/iovs/936793/ on 03/19/2018